ELSEVIER

Journal of Power Sources 4223 (2001) 1–9

JOURNAL OF POWER SOURCES

www.elsevier.com/locate/jpowsour

In situ studies of SEI formation

F. Kong[a], R. Kostecki[a], G. Nadeau[b], X. Song[a], K. Zaghib[b], K. Kinoshita[a,1], F. McLarnon[a,*]

[a]*Lawrence Berkeley National Laboratory, 1 Cyclotron Road, Berkeley, CA 94720, USA*
[b]*Institut de Recherche d'Hydro-Québec, 1800 boul Lionel-Boulet, Varennes, Qué., Canada J3X 1S1*

Received 16 June 2000; accepted 13 December 2000

Abstract

Electrolyte decomposition and the formation of a solid electrolyte interphase (SEI) layer occur during the initial charge/discharge cycles of carbon in electrolytes used in Li-ion batteries. This paper describes our approach to characterize the formation of SEI layers on various carbonaceous materials by in situ ellipsometry. Five types of carbon samples (carbon films on glass, pyrolyzed photoresist on silicon, highly oriented pyrolytic graphite and natural graphite) with specular surfaces were characterized by Raman spectroscopy and in situ ellipsometry/electrochemical studies in ethylene carbonate–dimethyl carbonate containing a lithium salt. Raman spectroscopy showed that the carbons films deposited on glass contain broad overlapping peaks from 900 to 1700 cm^{-1}, which is indicative of the highly disordered nature of the carbon films. Changes in the ellipsometric parameters, Δ and ψ, were correlated with the formation of the SEI layer during the initial charge (intercalation) process.

Keywords: Carbon; SEI layer; Ellipsometry; Raman spectroscopy; Li-ion batteries

1. Introduction

Both hard (non-graphitizable) and soft (graphitizable) carbonaceous materials are used in the negative electrodes for Li-ion cells. During the initial charge/discharge cycles, two chemical/electrochemical processes occur at the carbon electrode, namely, electrolyte decomposition and intercalation/deintercalation of Li^+ ions. Electrolyte decomposition and the formation of a solid electrolyte interphase (SEI) layer occur on the carbon surface at potentials more positive than that for Li^+ ion intercalation. The formation of the SEI layer is an irreversible reaction that is associated with a loss of cell capacity, hence it is commonly referred to as an irreversible capacity loss (ICL). Ideally, the SEI layer should form a passivating layer that is sufficiently compact to prevent the penetration of electrolyte and solvated Li compounds that contribute to ICL and possible exfoliation of the graphite structure. At the same time, the SEI layer should be sufficiently ionically conductive to permit reversible intercalation/deintercalation of Li^+ ions at suitable rates. When these conditions are met, stable performance and long cycle life are attained.

Characterization of the chemical composition and structure of the SEI is an ongoing topic of research. Aurbach and coworkers [1–6] used spectroscopic techniques to investigate the chemical composition of the SEI layer. A reaction product such as $(CH_2OCO_2Li)_2$ is formed on carbon in ethylene carbonate (EC)–dimethyl carbonate (DMC) and is reported to be an excellent passivating agent in the SEI layer. Studies by Yang et al. [7] indicate that the chemical components in the SEI layer vary with the solvent. In an electrolyte of pure EC, the passive film contains $(CH_2OCO_2Li)_2$, whereas in mixed solvents with DMC or diethyl carbonate (DEC), $C_2H_5OCOOLi$ and Li_2CO_3 are formed. Peled et al. [8] applied X-ray photoelectron spectroscopy, energy dispersive spectrometry, and scanning electron microscope techniques to analyze the SEI layer formed on the basal plane and cross-section of highly oriented pyrolytic graphite (HOPG) in 1 M $LiAsF_6$/EC–DEC (1.2). This study indicated that the SEI layer is thinner on the basal plane than on edge sites and its composition is different. The SEI formed on the edge sites is rich in inorganic compounds, whereas on the basal plane, it is rich in organic compounds. In addition, reduction of the solvent (EC and DEC) prevails on the basal plane, and reduction of the electrolyte salt ($LiAsF_6$) is the main contributor to SEI formation on the

* Corresponding author. Tel.: +1-510-486-4636; fax: +1-510-486-4260.
E-mail addresses: k_kinoshita@lbl.gov (K. Kinoshita), frmclarnon@lbl.gov (F. McLarnon).
[1] Tel.: +1-510-486-7389; fax: +1-510-486-4260.

0378-7753/01/$ – see front matter
PII: S0378-7753(01)00588-2

edge sites. Yazami [9] reported that electrolyte decomposition and the formation of polymerization products such as polyethylene oxide and polycarbonate resins occurred on carbon fibers in $LiPF_6$/EC. The resulting SEI layer consists of both inorganic and organic compounds.

Even though various electrochemical, spectroscopic and surface analytical techniques have been used to study the formation and growth of SEI layers, understanding of the relationships between the SEI layers, electrodes, electrolytes and dynamics is quite limited. This paper describes our approach to characterize the formation of SEI layers on various carbonaceous materials by in situ ellipsometry and other techniques. This investigation extends a preliminary study of SEI layer formation on pyrolyzed photoresist by in situ ellipsometry [10].

2. Experimental

Five types of carbon samples were used: (i) electron-beam (E-beam) evaporated carbon film on glass (Tufts University); (ii) F-beam carbon film on glass (International Crystal Manufacturing Co., ICM); (iii) HOPG (Advanced Ceramics Corp.); (iv) natural graphite powders (Hydro Quebec) with average particle size ranging from 2 to 40 μm and (v) pyrolyzed carbon films on silicon wafers produced in the microfabrication facility in the electronics research laboratory on the campus of the University of California at Berkeley [11]. The carbon surfaces were specular, except for the natural graphite powders. In this case, the powders were compressed in a die (2.54 cm diameter) at high pressures (∼50,000 psi) to form a thin disk with a smooth surface. The physicochemical properties of the carbon materials were characterized by Raman spectroscopy, atomic force microscopy (AFM) and spectroscopic ellipsometry.

A special test cell for in situ ellipsometry/electrochemical studies of carbon anodes in non-aqueous electrolytes was constructed. The polypropylene cell body was designed with a prismatic shape and openings for two optical windows, a working electrode, a counter electrode, and a reference electrode. This cell design avoided light refraction at the air/window/electrolyte interfaces, and thereby ensured that the probe beam was homogeneous (i.e. planes of constant phase and constant amplitude were parallel to each other and perpendicular to the beam propagation direction) along its path between the entering window and the carbon surface, provided that the optical signal encountered low loss in the electrolyte [12,13]. The probe beam intersected the normal plane of the carbon surface at an angle of incidence of 75°. The area of the working electrode was 2.8 cm^2, and its circumference was defined by the opening in the cell wall. A viton O-ring was used to seal the electrode to the polypropylene body, and the assembly was held with a screw clamp. The cell was assembled in a glove box, filled with electrolyte, sealed and then transferred to the ambient environment, where the electrochemical and ellipsometry data were obtained.

Raman spectroscopy measurements were carried out at room temperature in ambient atmosphere using an argon-ion laser (Coherent Inc. Model Innova 70) tuned to 514.5 nm and at 50 mW beam power. The resolution of this instrument is approximately 1.7 cm^{-1}. A commercial software package (PeakFit, version 4, AISN Software Inc.) that utilized baseline correction was used to deconvolute the Raman spectra. Ex situ AFM images were obtained with a molecular imaging (MI) scanning probe microscope coupled with a park scientific instruments (PSI) electronic controller using PSI MLCT-AUNM microlevers (0.05 N m^{-1}).

A self-compensating spectroscopic ellipsometer [14] was used to monitor in situ the film formation on the carbon surface. This instrument consisted of a polarizer–compensator-sample-analyzer layout, and two Faraday cells magnetically rotated the polarization azimuths of the probe beam, analogous to the mechanical rotation of polarizer and analyzer prisms. A rotating circular interference filter provided spectral scanning over the range 330–730 nm, and acquisition of an ellipsometric spectrum could be completed in a few seconds. For the study of transient phenomena, the temporal resolution of measurements was maximized by recording ellipsometric parameters at a single wavelength, which was 500 nm in this study. The overall uncertainties in ellipsometric measurements were estimated to be ∼0.025° for ψ and 0.05° for Δ. Interpretation of the observed ellipsometric data are based on the fundamental optics of polarized light propagation in stratified planar structures, as described elsewhere [15].

The ellipsometric parameters ψ and Δ were measured as the carbon electrode was scanned from its open circuit potential (∼3.0 V) to 0 V and then back to 3.5 V at 1–5 mV s^{-1}. The electrolyte was typically 1 M $LiPF_6$/EC–DMC (1:1) obtained from EM Industries Inc. (Selectipur Battery Electrolyte LP30) with a nominal water content <30 ppm. In some experiments with HOPG and the carbon films, 1 M $LiClO_4$/EC–DMC (1:1) was also used.

3. Results and discussion

3.1. Sample preparation

The E-bearn carbon films on glass and pyrolyzed carbon films on silicon were used for in situ ellipsometry/electrochemical studies without further preparation. A fresh surface of HOPG was obtained for the in situ studies by removing the outer basal plane layer with adhesive tape. The natural graphite powders were pressed without a binder into thin disks (∼1 mm in thickness) using a die in a hydraulic press. Problems encountered include graphite flakes stuck to the surface of the die pistons, inhomogeneity of the surface (i.e. visual appearance not uniform) and the presence of visible cracks in the disks. The best results were

obtained by pressing the powder in the die after carefully polishing the piston faces. These graphite disks had a density of 2 g cm^{-3} or about 88% of theoretical density. These samples were examined by ellipsometry, both in air to obtain the ellipsometric parameters of graphite and in the electrochemical cell. As will be mentioned later, we were not able to obtain meaningful in situ ellipsometry data with the natural graphite, because the disks were not mechanically stable in the electrochemical cells. Further experiments are underway to improve the physical integrity of the graphite disks.

3.2. Raman spectroscopy

Ex situ Raman spectra of four carbon samples are presented in Fig. 1. Typically, two major Raman peaks are observed with carbon, i.e. the D-band (~1355 cm^{-1}) and the G-band (E_{2g} C–C stretching band at 1580 cm^{-1}). These Raman peaks have been studied extensively as indicators of disorder in carbon materials [16–21]. The magnitude of the D/E_{2g} ratio usually correlates inversely with the microcrystalline size determined from X-ray diffraction analysis. In fact, the D/E_{2g} ratio increases with higher edge plane density, because of the breakdown of the ***k***-vector selection rule from reduced symmetry at the graphite edges. Thus, an increase in D/E_{2g} ratio is more related to graphitic edges than to microcrystallite size, although smaller microcrystallites naturally have a higher edge density. The Raman spectra shown in Fig. 1 fall into two separate groups, based on the spatial variation of the D/E_{2g} ratio. The spectra of freshly cleaved HOPG (Fig. 1a), and natural graphite (Fig. 1b) display a narrow E_{2g} band and a weak D-band. Based on the original D/E_{2g} ratio, correlation of Tuinstra and Koenig [18], our Raman data for HOPG indicate a crystallite size >1000 Å, whereas for natural graphite, the results indicate crystallites of ~180 Å.

The Raman spectra of the pyrolyzed carbon film (Fig. 1c) and electron-beam evaporated carbon film (Fig. 1d) exhibit more complex profiles. Two-band deconvolution of the spectra did not give sufficiently accurate results. We found that a four-Gaussian-peaks model was necessary to account for the observed Raman features. The Raman peaks at 1355, 1370, 1580 and 1622 cm^{-1} were deconvoluted from the spectrum of the pyrolyzed carbon (Fig. 1c). The peaks at 1355 and 1580 cm^{-1} can be identified with the carbon D and G bands. The proximity of the 1370 cm^{-1} peak to the D-band suggests a similar origin, but its slightly different position and large bandwidth may result from the carbon chain structure of the precursor photoresist. A second, first-order zone boundary phonon that appears at 1622 cm^{-1} is usually attributed to strongly altered surface layers. On the basis of available literature data [17,22,23], the band at 1622 cm^{-1} probably arises from oxidation-induced surface disorder of carbon.

The profile of the Raman spectrum of the electron-beam evaporated film (Fig. 1d) is the characteristic of an amorphous carbon with short-range order and multiphase structure. Peak deconvolution revealed the G- and D-bands at 1571 and 1353 cm^{-1}, respectively. Carbon structure models in which sp^3-bonded atoms with lower force constants are mixed into the sp^2 graphite lattice can explain the observed slight shift of the G-band to lower frequencies. Beside the D- and G-bands, band-fitting analysis unveiled two additional peaks at 1178 and 1482 cm^{-1}. According to the literature [23,24], the peak at 1178 cm^{-1} is assigned to a nanocrystalline diamond phase, and the peak at 1482 cm^{-1} peak is attributed to a diamond precursor phase.

Ex situ Raman spectra (see Fig. 2) were also obtained with carbon electrodes that were electrochemically cycled in 1 M $LiPF_6$/EC–DMC (1:1). After potential cycling, the electrodes were washed with DMC to remove residual electrolyte and $LiPF_6$, and then dried in a glove box. The

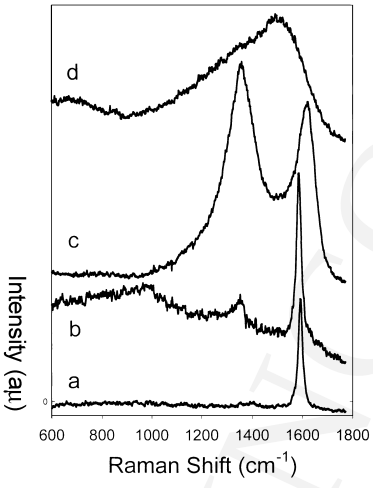

Fig. 1. Ex situ Raman spectra of carbon samples at 514.5 nm: (a) HOPG; (b) natural graphite; (c) pyrolyzed carbon film; (d) electron-beam evaporated carbon film.

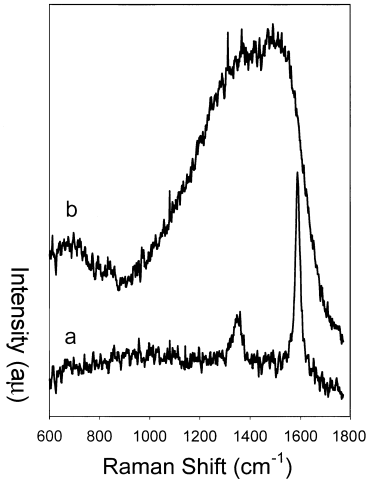

Fig. 2. Ex situ Raman spectra of (a) natural graphite and (b) electron-beam evaporated carbon film electrochemically cycled in 1 M $LiPF_6$/EC–DMC (1:1).

spectrum of natural graphite (Fig. 2a) shows G and D bands at positions identical to those observed in the spectrum of the original material. However, band fitting and band analysis revealed that the D/E_{2g} ratio increased slightly and that the calculated microcrystallite dimension L_a decreased to 103 Å. This value is 45% smaller than L_a for the as-received natural graphite, suggesting that electrochemical intercalation leads to the breakdown of graphite planes and introduces measurable disorder into the graphite-type material.

Deconvolution and band analysis of the Raman spectra (Fig. 2b) of electrochemically cycled evaporated carbon showed four peaks at positions very close to those observed for the freshly prepared film (Fig. 1d). However, comparison of the normalized intensity of each peak to the total intensity revealed a substantial increase in the D-band intensity. The relative enhancement of the D-band at 1355 cm^{-1} indicates a further increase in the structural disorder. The increase in the graphitic edge density was mainly due to the breakdown of graphite structure that is reflected by a significant decrease of the G-band intensity. The relative intensities of the two sp^3 diamond-type peaks also decreased, but to a lesser extent. It is difficult to determine the exact carbon structure by quantifying the contributions from the sp^3 and sp^2 Raman peaks. The relative contribution of σ over π electrons are difficult to ascertain due to the $\pi \rightarrow \pi^*$ enhanced resonance effect and to the different Raman scattering cross-sections of sp^3 and sp^2 carbon sites. However, we can conclude that the increase of the D-band intensity occurs with a decrease in both sp^2 and sp^3 sites.

3.3. Atomic force microscopy

Fig. 3 shows topographic AFM images of the evaporated carbon film and natural graphite recorded before and after electrochemical cycling in 1 M $LiPF_6$/EC–DMC (1:1). The freshly evaporated carbon film has a relatively smooth surface morphology that consists of tightly packed globular grains. The natural graphite shows clearly aligned graphite flakes with distinct edge planes. The images of both the evaporated carbon film and natural graphite after cycling show a dramatic change in the surface morphology, with a large increase in roughness and non-uniformity. In both

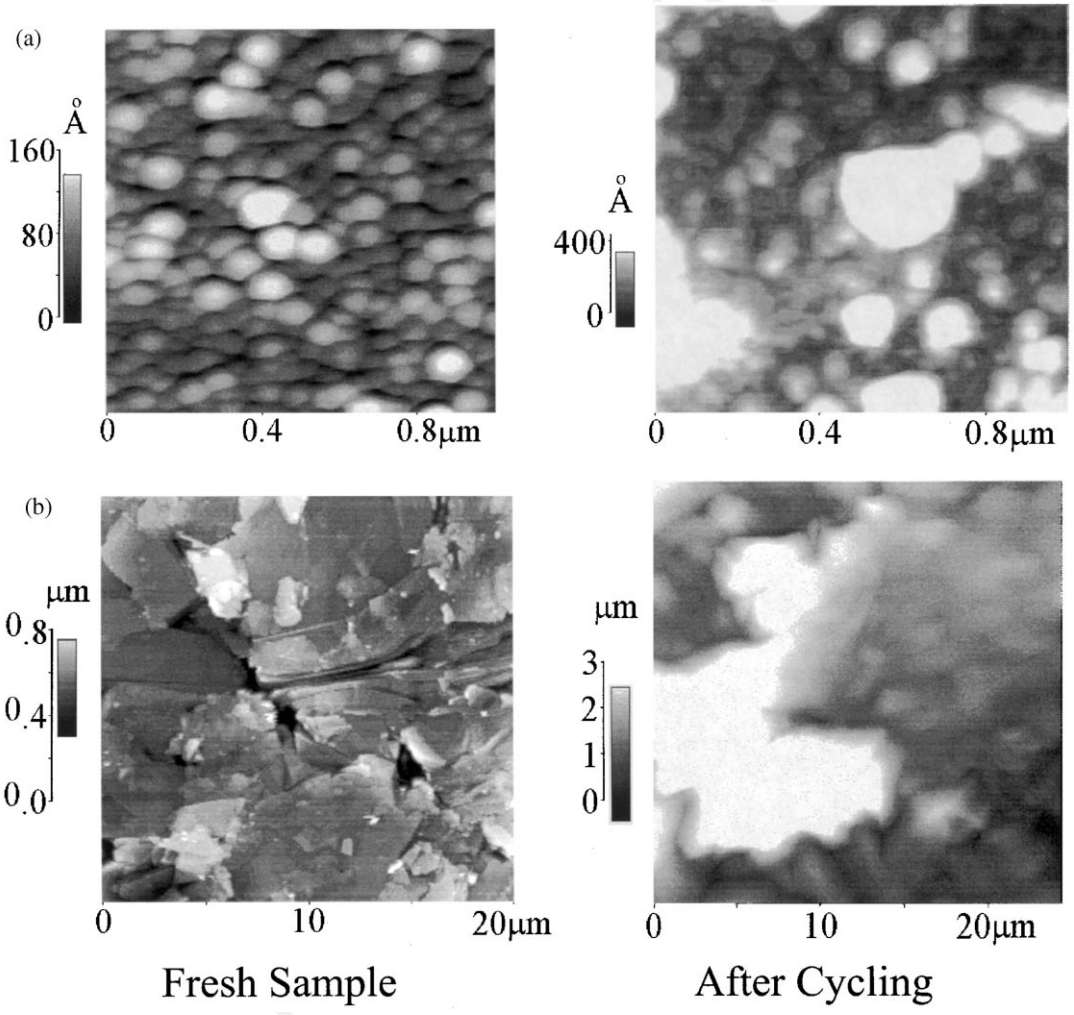

Fig. 3. Topographic AFM images of (a) evaporated carbon and (b) natural graphite before and after electrochemical cycling in 1 M $LiPF_6$/EC–DMC (1:1).

cases, surface roughness increases by an order of magnitude. Some of the particles grew substantially and protruded from the surface. This may be the result of uneven surface electrochemical activity that may result from the local changes of the carbon structure, mechanical breakdown of carbon particles or non-uniform thickness and composition of the SEI layer.

3.4. Electrochemical/ellipsometry measurements

The ellipsometric parameters, ψ and Δ, of the carbon samples were measured in air prior to the electrochemical experiments. This data and the apparent optical constants derived from modeling calculations are summarized in Table 1. The E-beam carbon films, which are about 100 nm thick, show a large variation in ellipsometric parameters, because of optical interference. A semi-infinite medium model was used for HOPG and natural graphite, and a single-layer model was used to analyze the results for carbon films. All of the carbon samples showed highly refractive, strongly absorbing, and optically non-dispersive behavior, in agreement with published results [25,26]. The relatively wide range of optical constants is indicative of the large differences in the crystalline structures and surface conditions of these carbon samples, which is consistent with Raman and AFM observations. These optical constants provide fundamental information on the optical compactness, surface roughness, and optical extinction related to absorbing or scattering effects, and for establishing a precise reference point for our in situ studies.

Our in situ experiments with the natural graphite disks were not successful, because they swelled or mechanically disintegrated when the potential was scanned from open circuit to 0 V. The swelling is believed to originate from penetration of electrolyte into the cracks and fissures present between the flake-like particles and/or expansion of the graphite structure by intercalation of Li^+ ions. Cyclic voltammetry (CV) of the carbon films obtained from Tufts University showed an anomalous current that precluded further studies of their ellipsometric parameters. A very high cathodic current was observed that rapidly decreased during the initial cathodic potential scan from open circuit, which is the opposite of the normal behavior observed with other carbons. We have no plausible explanation for the current response at this time.

The ellipsometric parameters and current–potential profiles for pyrolyzed carbon film (photoresist pyrolyzed at 1100°C), carbon film (ICM) and HOPG are presented in Figs. 4–6, respectively. Because the potential scan rates were different for each of the carbons, and because the surface structures of the carbons are different, we made no attempt to compare the current–potential profiles in Fig. 4a to Fig. 6a. The initial current–potential profiles in Fig. 4a to Fig. 6a showed evidence for cathodic currents that are attributed to electrolyte decomposition and formation of SEI layers during the potential scans from open circuit to 0 V [1–10]. The current–potential profiles for the pyrolyzed carbon film and carbon film (ICM) in Fig. 4a and Fig. 5a, respectively, showed several broad, overlapping current peaks at potentials >0.4 V. The HOPG (see Fig. 6a) showed a considerably more complex current–potential profile during CV. Some small structures appeared in the CV curves when the cathodic sweep reached ~1.5 V, and one or two strong dips typically appeared at ~0.4 V. Interestingly, the dip(s) at ~0.4 V reappeared in the anodic potential sweep. This behavior can be attributed to a cascade mass transfer process of Li^+ ion intercalation, solvated-Li compound intercalation, or continuing electrolyte decomposition reactions.

The corresponding ellipsometric parameters obtained at a wavelength of 500 nm during the initial cathodic scan from open circuit potential to 0 V are presented in Fig. 4b to Fig. 6b. The ellipsometry data indicate that variations in ψ and Δ are associated with the formation of the SEI layer and electrolyte decomposition during the initial cathodic scan. The potential at which the parameters changed, and the magnitude of the change, varied with the carbon sample. For example, ψ and Δ increased by ~3 and 10°, respectively, when the potential of the pyrolyzed carbon film (produced at 1100°C) reached about 1.5 V. The optical constant n decreased (i.e. corresponding to an increase in ψ), indicating that the SEI layer is optically less compact than the carbon film. The ellipsometric parameter, ψ changed almost linearly from ~18 to ~27° and Δ increased ~5° during the cathodic scan of the carbon film (ICM) between 1.25 and 0 V. The large increase in the ellipsometric parameters, especially ψ is attributed to increasing roughness of the carbon surface. This conclusion agrees with the analysis of the AFM measurement of the carbon film (ICM) which showed increased roughness upon cycling.

Table 1
Ellipsometric parameters and optical constants of carbon

Carbon samples	Ellipsometric parameters		Apparent optical constants	
	ψ (°)	Δ (°)	n	k
E-beam evaporated carbon (Tufts University)	12–22	35–80	2.0–2.8	1.1
E-beam evaporated carbon (ICM)	12–24	40–90	1.9–3.1	1.4
HOPG	15–17	85–93	3.1–3.2	1.7–2.2
Natural graphite	16.5–17.5	60–64	2.5–2.6	1.2–1.4
Pyrolyzed carbon film	23–27	33–37	1.5–1.8	0.7–0.8

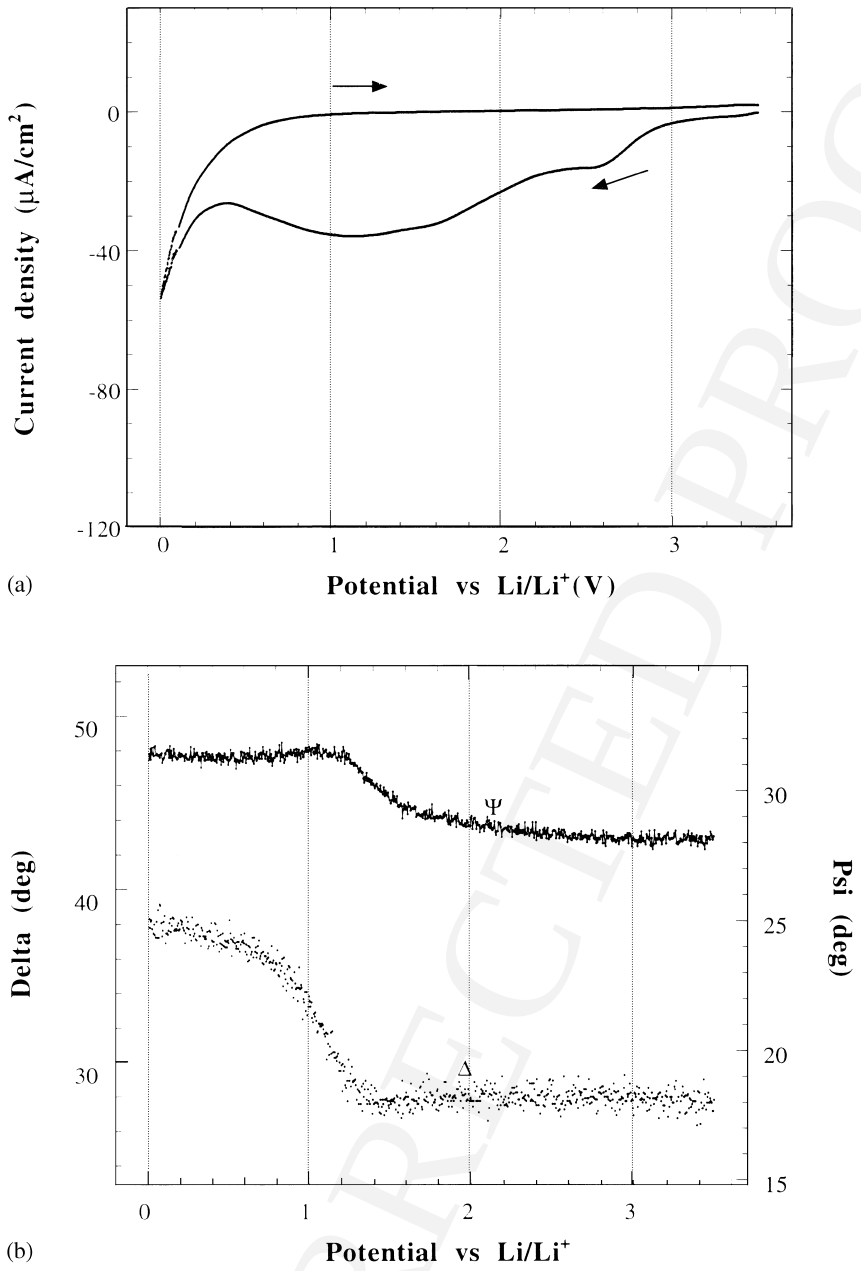

Fig. 4. In situ ellipsometry/electrochemical studies of pyrolyzed photoresist carbon film in 1 M $LiPF_6$/EC–DMC (1:1): (a) potential scan rate 5 mV s^{-1}; (b) ellipsometric data were obtained at 500 nm.

With HOPG, the dominant surface that is exposed to the electrolyte is the basal plane, with some edge sites present at grain boundaries and defects. The values of ψ and Δ observed by in situ ellipsometry (see Fig. 6b) also exhibited perceptible changes, but at a more cathodic potential of about 0.4 V in 1 M $LiPF_6$/EC–DMC (1:1). These results confirm that the SEI layer is formed at the basal plane surface, and is consistent with the conclusions of other studies [27,28] which reported electrolyte decomposition on both the basal and edge planes.

Fig. 7 shows the ellipsometric data obtained at 500 nm with a carbon film (ICM) during the first three potential cycles between 2.0 and 0 V. The first cycle shows the same ellipsometric data between 2 and 0 V as those presented in Fig. 5b. After the initial formation of the SEI layer and the corresponding large change in ψ and Δ, the parameter ψ shows a small decrease, while Δ remains nearly constant, as the potential changes from 0 to 2 V. The smaller variations in ψ and Δ after the initial formation of the SEI layer are related to compositional changes, surface modifications (i.e. expansion/contraction) as Li^+ ions intercalate and deintercalate, and a slight increase of the SEI layer thickness during potential cycling. When the potential is scanned cathodically, Li^+ ions intercalate to form a lithiated carbon and the

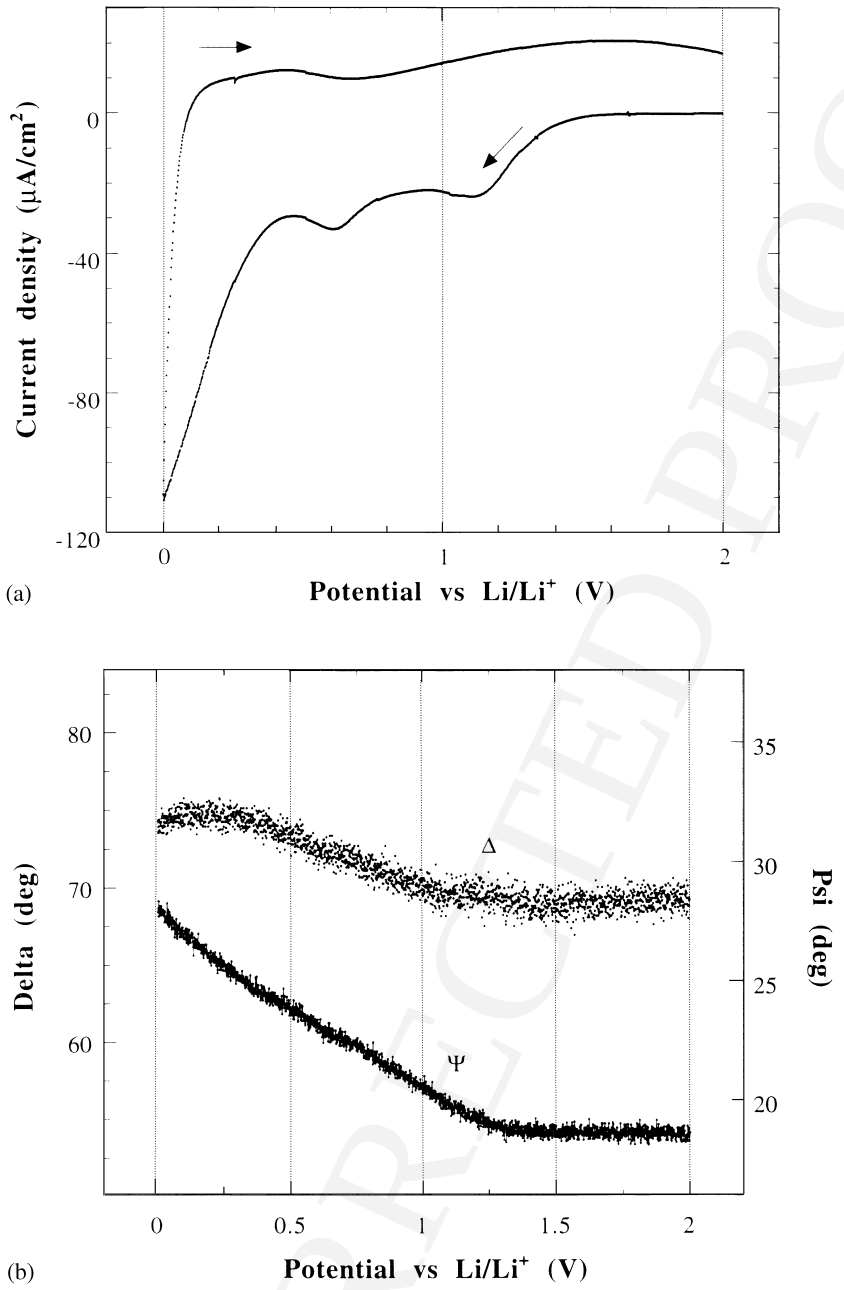

Fig. 5. In situ ellipsometry/electrochemical studies of carbon film (ICM) in 1 M $LiClO_4$/EC–DMC (1:1): (a) potential scan rate 1 mV s^{-1}; (b) ellipsometric data were obtained at 500 nm.

crystalline structure expands. The optical properties of the lithiated carbon are different from those of the carbon film with a SEI layer, and thus the ellipsometric parameters, ψ and Δ, vary accordingly. During the anodic potential scan, Li^+ ions leave the lithiated carbon (deintercalate) and the structure contracts, with ψ and Δ trending to values that correspond closely to carbon with a SEI layer.

Optical modeling of the ellipsometric data indicated that the changes in ψ and Δ reflect changes in the compactness and apparent absorption of the surface layer. Full ellipsometric spectra (330–730 nm) were measured before and after the potential cycles of the carbon film (ICM) and are shown in Fig. 8. Two optical models, one which considered the surface roughness of the carbon film and the other excluding surface roughness were used in simulation calculations. The best fit of the experimental data suggested that a 60 nm thick homogeneous SEI layer was formed after the first potential cycle. A refractive index $n \sim 1.41$–1.52 and an extinction coefficient of $k \sim 0$, representing a medium, i.e. optically denser than common polymers and electronically non-conductive, were obtained from the analysis. Complete spectral measurements were also made after the

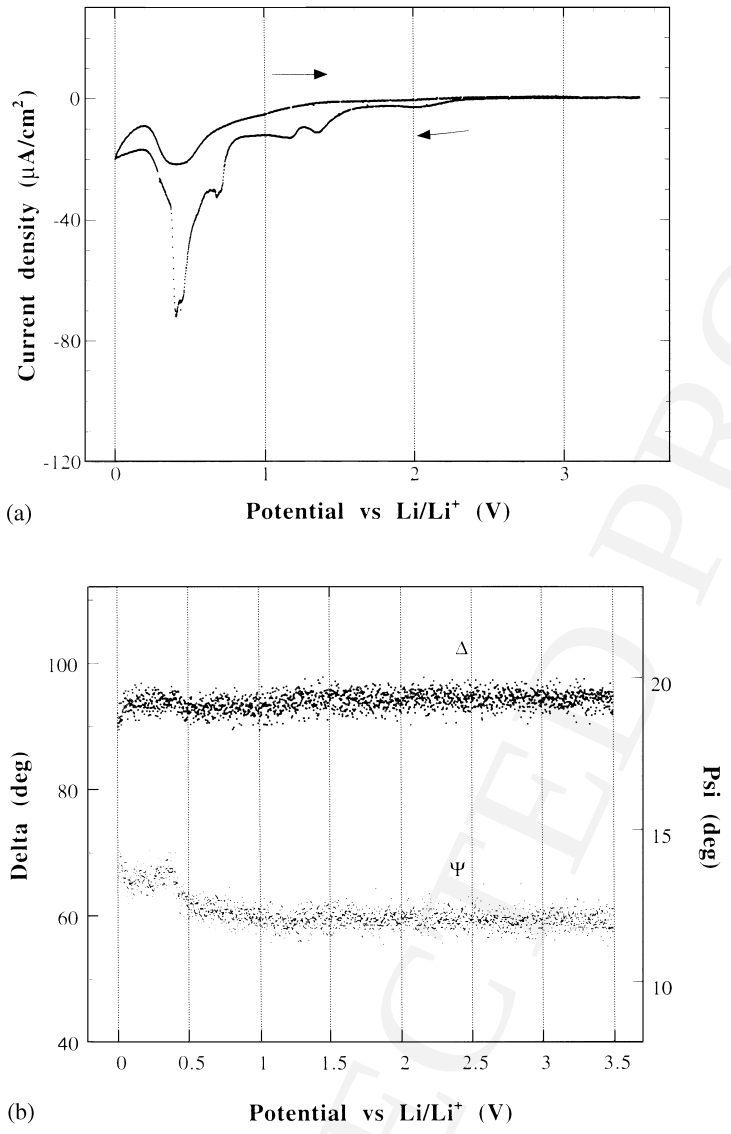

Fig. 6. In situ ellipsometry/electrochemical studies of HOPG (basal plane) in 1 M $LiPF_6$/EC–DMC (1:1): (a) potential scan rate 2 mV s^{-1}; (b) ellipsornetric data were obtained at 500 nm.

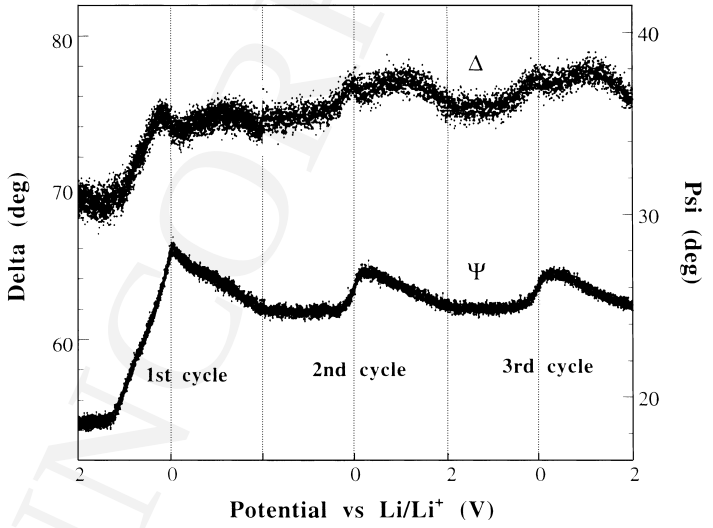

Fig. 7. In situ ellipsometric parameters obtained with carbon film (ICM) in 1 M $LiClO_4$/EC–DMC (1:1) during the first three potential cycles: (a) potential scan rate 1 mV s^{-1}; (b) ellipsometric data were obtained at 500 nm.

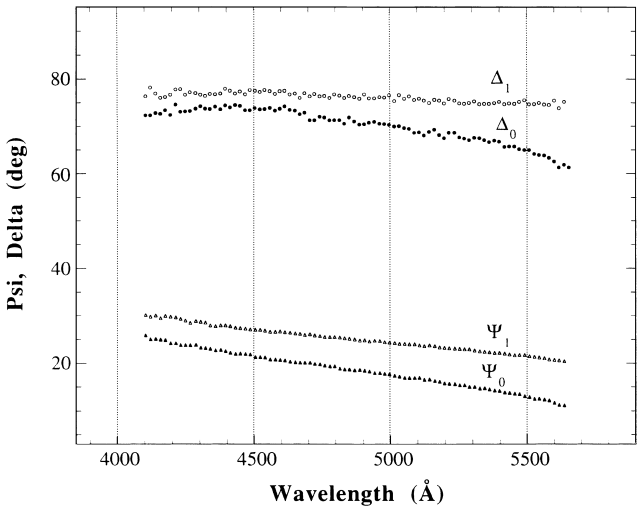

Fig. 8. Ellipsometric spectra (330–730 nm) of the carbon film (ICM) before (subscript = 0) and after (subscript = 1) the first potential cycle in 1 M $LiClO_4$/EC–DMC (1:1).

third and seventh potential cycles, and the analysis indicated that the SEI layer thickness was the same as that after the first potential cycle. Complementary studies with an electrochemical quartz crystal microbalance are underway to determine mass changes to the SEI layer on evaporated carbon films during potential cycling [29]. Ellipsometric spectra of the HOPG surface before and after the first two cycles indicate the formation of a SEI layer, i.e. 36 nm thick, containing mostly LiF and smaller amounts of organic material. A detailed discussion of the ellipsometric data is outside the scope of this paper, but will be addressed in a subsequent publication when additional results are obtained.

In conclusion, in situ ellipsometry provides a sensitive technique to observe SEI layer formation and growth during charge/discharge cycling. Raman spectroscopy clearly showed that the structures of the different carbon samples varied significantly. AFM measurements showed that the graphite surface roughness changed dramatically during intercalation of Li^+ ions. This observation was corroborated by Raman and ellipsometry studies of carbon that was electrochemically cycled. When these studies are complemented by other analytical measurements, additional information on the properties of the SEI layer can be obtained.

Acknowledgements

This work was supported by Hydro Quebec and the Assistant Secretary for Energy Efficiency and Renewable Energy, Office of Transportation Technologies, Office of Advanced Automotive Technologies of the US Department of Energy under contract No. DE-AC03-76SF00098 at Lawrence Berkeley National Laboratory. The authors would like to thank R. Goldner and N. Clay of Tufts University (Medford, MA) for kindly supplying carbon films used in this study.

References

[1] D. Aurbach, Y. Ein-Eli, O. Chusid, Y. Carmeli, M. Babai, H. Yamin, J. Electrochem. Soc. 141 (1994) 603.
[2] D. Aurbach, Y. Ein-Eli, B. Markovsky, A. Zaban, S. Luski, Y. Carmeli, H. Yamin, J. Electrochem. Soc. 142 (1995) 2882.
[3] D. Aurbach, B. Markovsky, A. Shechter, Y. Ein-Eli, H. Cohen, J. Electrochem. Soc. 143 (1996) 3809.
[4] D. Aurbach, B. Markovsky, I. Weissman, E. Levi, Y. Ein-Eli, Electrochim. Acta 45 (1999) 67.
[5] D. Aurbach, A. Zaban, Y. Ein-Eli, I. Weissman, O. Chusid, B. Markovsky, M. Levi, E. Levi, A. Shechter, E. Granot, J. Power Sources 68 (1997) 91.
[6] O. Chusid, Y. Ely, D. Aurbach, M. Babai, Y. Carmeli, J. Power Sources 43 (1993) 47.
[7] C. Yang, Y. Wang, C. Wan, J. Power Sources 72 (1998) 66.
[8] D. BarTow, E. Peled, L. Burstein, J. Electrochem. Soc. 146 (1999) 824.
[9] R. Yazami, Electrochim. Acta 45 (1999) 87.
[10] F. Kong, J. Kim, X. Song, M. Inaba, K. Kinoshita, F. McLarnon, Electrochem. Solid State Lett. 1 (1998) 39.
[11] J. Kim, X. Song, K. Kinoshita, M. Madou, R. White, J. Electrochem. Soc. 145 (1998) 2314.
[12] J.M. Stone, Radiation and Optics, McGraw-Hill, New York, 1963 (Chapters 15 and 16).
[13] R.H. Muller, Surf. Sci. 16 (1969) 14.
[14] R. Muller, J. Farmer, Rev. Sci. Instrum. 55 (1984) 371.
[15] R.M.A. Azzam, N.M. Bashara, Ellipsometry and Polarized Light, North-Holland, New York, 1977.
[16] K. Kinoshita, Carbon: Electrochemical and Physicochemical Properties, Wiley, New York, 1988.
[17] R. Bowling, R. Packard, R.L. McCreery, J. Am. Chem. Soc. 111 (1989) 1217.
[18] G. Katagiri, H. Ishida, A. Ishitani, Carbon 26 (1988) 565.
[19] K. Ray, R.L. McCreery, Anal. Chem. 69 (1997) 4680.
[20] F. Tuinstra, J.L. Koenig, J. Chem. Phys. 53 (1970) 1126.
[21] M. Nakamizo, K. Tamai, Carbon 22 (1984) 197.
[22] M.S. Dresseihaus, G. Dresselhaus, Adv. Phys. 30 (1981) 139.
[23] J. Schwan, S. Ulrich, V. Batori, H. Ehrhardt, S.R.P. Silva, J. Appl. Phys. 80 (1996) 440.
[24] J. Hong, A. Goullet, G. Turban, Thin Solid Films 352 (1999) 41.
[25] A. Borghesi, G. Guizzetti, in: E.D. Palik (Ed.), Handbook of Optical Constants of Solids II, Academic Press, New York, 1998, pp. 449–460.
[26] C. Barbero, R. Kotz, J. Electrochem. Soc. 140 (1993) 1.
[27] G.-C. Chung, S.-H. Jun, K.-Y. Lee, M.-H. Kim, J. Electrochem. Soc. 146 (1999) 1664.
[28] G. Nadeau, K. Zaghib, K. Kinoshita, J. Electrochem. Soc., in press.
[29] J. Evans et al., University of California at Berkeley, 2000, unpublished data.